High-purity and narrow-band red fluorescence in Er^{3+}/Yb^{3+} co-doped Bi_2O_3 nano-powder

CHENGGUO MING[1,*], QIMING XIA[1], AIHUA ZHOU[1], YUANXUE CAI[1], XIAOXU CHEN[1], FENG SONG[2]
[1]*School of Science, Tianjin University of Science & Technology, Tianjin, 300457, China*
[2]*The Key Laboratory of Weak Light Nonlinear Photonics, Ministry of Education, Nankai University, Tianjin, 300457, China*

Up-conversion emissions located at low-absorption window (650-950 nm) of biological tissue is worthy of research for fluorescent probes, which was expected to have a high penetration depth. Our Bi_2O_3 nano-powders doped with Er^{3+} and Yb^{3+} ions can emit strong red up-conversion emission (peak at ~678 nm) under 980 nm excitation. And the color-purity (C-P) and full width half maximum (H-W) of the emission are ~0.99 and 31 nm for sample Bi4 at lower pumping power (373 mW), which can bring a high signal-noise-ratio. This study is greatly helpful in exploring fluorescent materials for internal tissue imaging.

(Received March 26, 2025; accepted October 10, 2025)

Keywords: Optical materials and properties, Luminescence, Nanoparticles

1. Introduction

In recent years, up-conversion fluorescence materials have specially attracted people's attention because of their lots of advantages, including low fluorescence bleaching, tunable fluorescence wavelength, high chemical stability, good biological compatibility, and stronger fluorescence intensity, and so on [1-6]. To obtain excellent up-conversion fluorescence materials, the luminous center and the matrix component are two crucial intrinsic factors. As luminous center, trivalent lanthanide ions (like as Er^{3+}, Tm^{3+}, Eu^{3+}, Tb^{3+}, Ho^{3+}, Sm^{3+}, Dy^{3+}, Pr^{3+} and Nd^{3+}) have abundant absorption and emission spectra in the visible and infrared wavelength region. Especially, these ions can emit strong up-conversion visible light under infrared excitation, which have many advantages, such as the narrow emitting band, long fluorescence lifetime, and less background interference. The fluorescent characteristics of the luminous ion are related to the matrix component. The same luminous ion doped in different host materials can display different fluorescent characteristic. The phonon energy, crystal field structure, and thermal stability of the host material are the mainly factors. The trivalent Er^{3+} ion can emit strong up-conversion green ($^4S_{3/2}/^2H_{11/2}\rightarrow{}^4I_{15/2}$) and red ($^4F_{9/2}\rightarrow{}^4I_{15/2}$) emissions under infrared excitation [7-12]. The Yb^{3+} trivalent ion has a larger absorption cross section for the 980 nm excitation light, and its $^2F_{5/2}$ energy level closely matches the $^4I_{11/2}$ energy level of the Er^{3+} ion. Thus, in this work, the Er^{3+} and Yb^{3+} ion were chosen as the activator and sensibilizer, respectively. In view of the low-absorption of biological tissue in the 650-950 nm wavelength region [13-15], we studied Er^{3+}/Yb^{3+} co-doped Bi_2O_3 nanopowders and attempted to obtain strong up-conversion emission at this band.

2. Experiment and method

2.1. Preparation

Bismuth nitrate pentahydrate ($Bi(NO_3)_3\cdot5H_2O$, ≥99.99%, metals basis), Erbium trinitrate pentahydrate ($Er(NO_3)_3\cdot5H_2O$, ≥99.9%, metals basis), and Ytterbium trinitrate pentahydrate ($Yb(NO_3)_3\cdot5H_2O$, ≥99.9%, metals basis) were chosen as the raw materials.

2.2. Experimental procedure

The nano-powders with the constituents of $(95\text{-}x)Bi_2O_3\text{-}0.25Er_2O_3\text{-}xYb_2O_3$ (mol%) were synthesized by complex sol-gel method. The samples with x=1, 1.5, 2, 2.5, and 3 were prepared and marked as Bi1, Bi2, Bi3, Bi4, and Bi5, respectively. The detail preparation process can be referred in reference [16].

2.3. Measurements

Using a 980 nm laser diode as excitation source, the luminescence spectra were obtained by employing a luminescence spectrometer (HORIBA Fluorolog-3). The X-ray diffraction (XRD) of the samples was obtained using a Bruker AXSB8 Discover. All measures were taken in room temperature.

3. Results and discussion

The XRD of the all samples had been measured. The profile and shape of spectral line are no difference, and the location and intensity of diffraction peak are also the same. The XRD diagram of the Bi4 sample was shown in Fig. 1. By comparing with the standard card: 27-0052, the groups of the sharp diffraction peaks should be from Bi_2O_3, whose oxide lattice is a cubic system, and its space group is Pn3m (224). Based on the Scherer's formula:

$$d_{hkl} = k\lambda / \beta \cos\theta \quad (1)$$

where d_{hkl}, K, λ, β, and θ present the crystal size in the vertical direction of (hkl), a constant (0.9), the wavelength of X-ray radiation (0.154 nm), the full width half maximum of the diffraction peak, and the angle of diffraction. The size of Bi_2O_3 nanocrystal was calculated by using the (111) diffraction, whose value is about 180 nm.

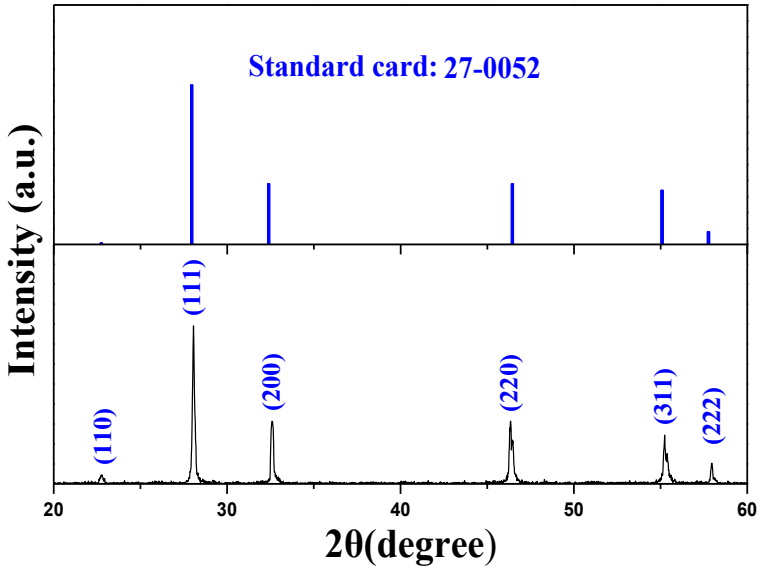

Fig. 1. XRD diagram of the Bi4 sample (down-figure), and the standard diagram coming from the PDF card:27-0052 (above-figure) (colour online)

Under 980 nm excitation (power: 373 mW), up-conversion emissions of the Er^{3+}/Yb^{3+} co-doped Bi_2O_3 nano-powders with different Yb^{3+} doping concentration were measured. The spectral diagram of the Bi1, Bi2, Bi3, Bi4, and Bi5 samples are shown in Fig. 2. The spectral profile and peak location of the up-conversion emissions for Bi1, Bi2, Bi3, Bi4, and Bi5 samples samples are the same, except for the intensity of the up-conversion emission. With the increase of the Yb^{3+} ion concentration, the red up-conversion emission ($^4F_{9/2} \rightarrow {}^4I_{15/2}$) firstly increase and then decrease. The luminescence intensity of the Bi4 sample (doping 2.5 mol% Yb^{3+}) is largest. Fig. 3 is power spectra of the Bi4 sample, whose pumping power is 65, 126, 188, 250, 321, 373, 415, 479, and 525 mW, respectively. The green up-conversion emission at 520-560 nm is very weak, almost undetectable, which should be due to the transition of Er^{3+} ion from $^4S_{3/2}(^2H_{11/2})$ to $^4I_{15/2}$. However, strong red up-conversion emission located at 630-700 nm was observed, which should be from the transition of Er^{3+} ion from $^4F_{9/2}$ to $^4I_{15/2}$.

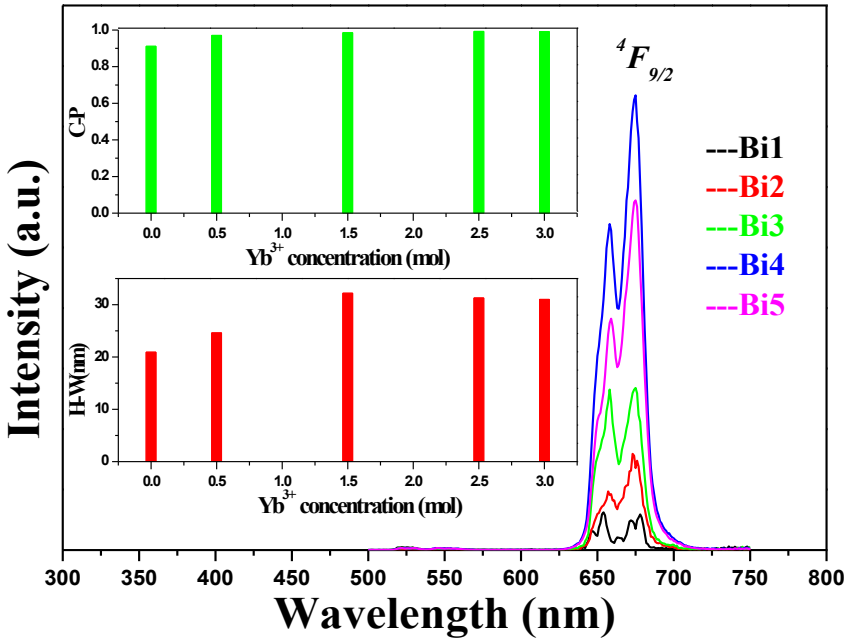

Fig. 2. Up-conversion spectra of the Bi1-Bi5 samples under 980 nm excitation (power: 373 mW); the inset is color-purity (C-P) and full width at half-maximum (H-W) of the red emission (Er^{3+}: $^4F_{9/2}\rightarrow{}^4I_{15/2}$) vs Yb^{3+} ion concentration (colour online)

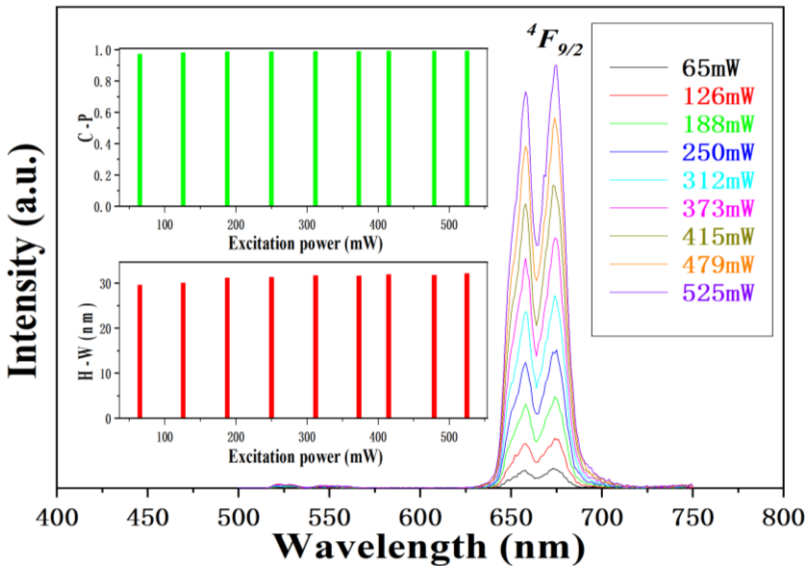

Fig. 3. Power spectra of the Bi4 sample; the inset is Log-log curve of the red emission (Er^{3+}: $^4F_{9/2}\rightarrow{}^4I_{15/2}$) intensity vs excitation power (colour online)

The luminescence color-purity(*C-P*) is defined as:

$$C\text{-}P=I_1/I_2 \tag{2}$$

where I_1 and I_2 are the intensities of the signal luminescence and the whole luminescence. Larger the *C-P* value, better monochromaticity the luminescence has. The *C-P* values under different excitation power were calculated, and the relationship between the color-purity and the excitation power is shown in the insets of Fig. 2 and Fig. 3. It is very obvious that the *C-P* becomes larger and larger with increase of Yb^{3+} ion concentration, and the maximum value appears in the bigger Yb^{3+} concentration (2.5 mol%), seen in the inset of Fig. 2. It is the same for *C-P* vs excitation power, the optimal excitation power is 479 mW, seen in the inset of Fig. 3. The maximum value of *C-P* value is close to 0.99, which indicates the better monochromaticity of the red luminescence ($^4F_{9/2}\rightarrow{}^4I_{15/2}$).

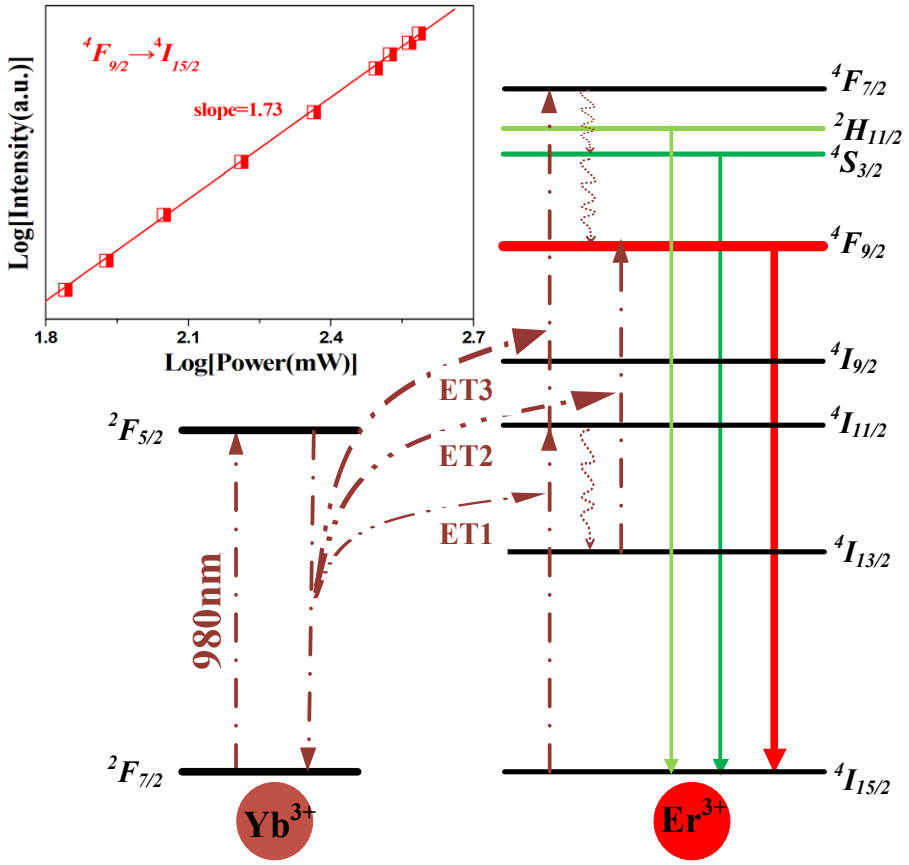

Fig. 4. Energy diagram of Er^{3+} and Yb^{3+} ions, as well as the potential population processes of the up-conversion emission (ET: energy transition); the inset is Log-log curve of the excitation power vs the intensity of the red luminescence (Er^{3+}: $^4F_{9/2}\rightarrow{}^4I_{15/2}$) (colour online)

Based on the relationship between pump power and luminescence intensity:

$$I \propto P^n \tag{3}$$

where I, P, and n are the intensity of up-conversion emission, excitation power of the excitation source, and absorbed excitation-photon counts for emitting one emission-photon, respectively. The inset of Fig. 4 is the Log-log curve of the red emission intensity vs excitation power. The value of n is 1.73, which shows the two-photon population process for the red up-conversion emission.

Fig. 4 is energy diagram of Er^{3+} and Yb^{3+} ions, as well as the potential population processes of the green and red up-conversion emission. Considering larger absorption cross of Yb^{3+} ion to 980 nm excitation emission, the directly absorption of Er^{3+} ion to the 980 excitation has been ignore, like as ground state absorption and excited state absorption. The population processes of green and red up-conversion emission can be described as follows. Firstly, Yb^{3+} ion are excited to $^2F_{5/2}$ state by absorbing one 980 nm photon. Secondly, the Yb^{3+} ion comes back the ground state ($^2F_{7/2}$), and transfers the energy to Er^{3+} ion by energy transition (ET) 1: ($^2F_{5/2}\rightarrow{}^2F_{7/2}$)-($^4I_{15/2}\rightarrow{}^4I_{11/2}$). Subsequently, by ET2: ($^2F_{5/2}\rightarrow{}^2F_{7/2}$)-($^4I_{11/2}\rightarrow{}^4F_{7/2}$) and ET3: ($^2F_{5/2}\rightarrow{}^2F_{7/2}$)-($^4I_{13/2}\rightarrow{}^4F_{9/2}$), the Er^{3+} ions are excited to $^4F_{7/2}$ and $^4F_{9/2}$ states, respectively. Finally, the Er^{3+} ions transfer $^4F_{7/2}$ from to $^4S_{3/2}$($^2H_{11/2}$) states by nonradiative transition. In the above population processes, the ET2 is very weak, but ET3 is very strong, which cause the weak green emission and very strong red emission. The reason should be the nonradiative transition from $^4I_{11/2}$ to $^4I_{13/2}$ state is very efficient, which increases the populations of $^4I_{13/2}$ state, and decreases the population of $^4I_{11/2}$ state.

4. Conclusions

The Er^{3+}/Yb^{3+} co-doped Bi_2O_3 nano-powders were prepared by high-temperature solid state reaction. The raw materials were sintered at 1200 °C for 6 hours in the air. The crystal size of the obtained powders is about 180 nm based on Scherer's formula. The oxide lattice is a cubic system. Under 980 nm excitation, the Er^{3+}/Yb^{3+} co-doped Bi_2O_3 nano-powders can emit strong red up-conversion emission, which comes from the transition of the Er^{3+} ion

from $^4F_{9/2}$ to $^4I_{15/2}$. The red emission displays better optical characteristics, whose color-purity (C-P) and full width half maximum (H-W) are ~0.99 and ~31 nm for sample Bi4 (Yb^{3+} doping concentration: 2.5 mol%) at lower pumping power (373 mW). In a word, our material is advantageous to develop fluorescent probe for internal tissue imaging, such as strong light penetrability, high color purity, and narrow bandwidth.

Acknowledgement

This work was supported by the National Natural Science Foundation of China (Grant No. 12174206), the National Key R&D Plan (Grant No. 2021YFB3502701).

Funding

This research was not funded.

Conflict of interest

The authors declare no conflicts of interest.

References

[1] G. Yi, G. Chow, Advanced Functional Materials **16**, 2324 (2010).
[2] X. Song, J. Yang, S. Wang, J. Song, B. Bao, H. Zhu, D. Yan, C. Xu, Y. Liu, Optical Materials **154**, 115774 (2024).
[3] L. Wang, N. Zhao, C. Zhu, L. Chen, Y. Jiang, R. Zhou, Y. Liu, B. Qu, H. T. Hintzen, Chemical Engineering Journal **483**, 149361 (2024).
[4] J. He, B. Wang, C. Gong, X. Wang, Q. Wang, J. G. Li, Optical Materials **157**, 116127 (2024).
[5] H. Q. Wang, M. Batentschuk, A. Osvet, L. Pinna, C. J. Brabec, Advanced Materials **23**, 26752680 (2011).
[6] R. Yan, Y. Li, Advanced Functional Materials **15**, 763 (2010).
[7] T. Wu, Y. Hong, L. Song, Y. Zhu, J. Wang, Y. Zhu, J. Fang, G. Chen, Optical Materials **124**, 111 (2022).
[8] X. Yang, Z. Wu, Z. Yang, X. Zhao, C. Song, M. Yuan, K. Han, H. Wang, S. Li, X. Xu, Journal of Alloys and Compounds **854**, 157 (2021).
[9] A. Zhou, F. Song, Y. Han, Song, D. Ju, X. Wang, CrystEngComm **20**, 2029 (2018).
[10] X. Luo, W. Zhao, Q. Chen, M. Zhi, Journal of Alloys and Compounds **897**, 162672 (2022).
[11] M. Runowski, S. Goderski, D. Przybylska, T. Grzyb, S. Lis, I. R. Martín, ACS Nano **3**, 6406 (2020).
[12] Z. Liu, F. Pu, S. Huang, Q. Yuan, J. Ren, X. Qu, Biomaterials **34**, 1712 (2012).
[13] C. S. Lobo, V. A. Tomé, F. A. Schaberle, M. J. F. Calvete, M. M. Pereira, C. Serpa, L. G. Arnaut, Inorganica Chimica Acta **514**, 119993 (2021).
[14] L. Wang, W. Du, Z. Hu, K. Uvdal, L. Li, W. Huang, Angewandte Chemie International Edition **58**, 14026 (2019).
[15] Z. Kyryl, C. W. Warren, Nature Materials **12**, 285 (2013).
[16] C. Ming, M. Pei, X. Ren, N. Xie, Y. Cai, Y. Qin, F. Yuan, G. Wang, L. An, F. Song, Materials Letters **218**, 154 (2018).

*Corresponding author: mingchengguo1978@163.com